Variation of Fluorescence Lifetimes and Judd-Ofelt Parameters between Eu^{3+} Doped Bulk and Nanocrystalline Cubic Lu_2O_3

J. C. Boyer,[†] F. Vetrone,[†] J. A. Capobianco,*[,†] A. Speghini,[‡] and M. Bettinelli[‡]

Department of Chemistry and Biochemistry, Concordia University, 7141 Sherbrooke St. W., Montreal, Canada, and Dipartimento Scientifico e Tecnologico, Università di Verona, and INSTM, UdR Verona, Ca' Vignal, Strada Le Grazie 15, I-37134 Verona, Italy

Received: May 6, 2004; In Final Form: September 13, 2004

The luminescent properties of 1 mol % Eu^{3+}-doped cubic Lu_2O_3 nanocrystals prepared by a combustion synthesis route were investigated. The visible emission spectrum of the europium doped Lu_2O_3 nanocrystals indicate that the structural environment surrounding the dopant Eu^{3+} ion is distorted when compared to a bulk sample with a micrometer particle size. From the resulting emission spectra, the Ω_2 and Ω_4 Judd-Ofelt intensity parameters were calculated. The lifetimes of the $^5D_0$ excited state for both the C_2 and C_{3i} sites were found to be nearly double that found for a similarly doped sample with larger particle size (bulk sample). This behavior is attributed to a change in the refractive index of the nanocrystalline material that in turn modifies the oscillator strength of the 4f ↔ 4f transitions.

1. Introduction

Over the past several years, there has been an ongoing search for nanometer sized powered phosphors with superior performance characteristics over their micrometer counterparts. This research has been stimulated by the fact that significant changes in the optical properties have been observed with decreasing particle size.[1] Currently, phosphors in the micrometer size range find applications in a wide variety of information display devices such as cathode-ray tubes (CRTs), field emission displays (FEDs), vacuum fluorescent displays (VFDs), and electroluminescent (EL) devices.[2] It is anticipated that the advent of nanosized phosphors could lead not only to improved resolution in these devices but also to an increase in luminescent efficiency. Research in the realms of nanocrystalline phosphors ranges from band gap semiconductors to lanthanide-doped insulators such as the common red phosphor Eu^{3+} doped Y_2O_3.

Nanocrystalline materials are usually defined as polycrystalline solids with particle diameters or grain sizes less than 100 nm.[3] Particle-size-dependent phenomena have been noted in several materials. The properties affected are (i) emission lifetime, (ii) luminescence efficiency, and (iii) concentration quenching. Recently, numerous studies have focused on the optical properties of nano-dimensioned Y_2O_3:Eu^{3+}. In particular, Tissue et al. have thoroughly investigated and reported results on Eu^{3+} doped monoclinic Y_2O_3 noting changes in the luminescent spectra and lifetime of the red $^5D_0 \rightarrow {}^7F_2$ transition with decreasing particle size.[1,3−5]

Over the past few years, our research groups have examined the spectroscopic and upconversion properties of lanthanide doped nanocrystalline cubic Y_2O_3.[6−8] Recently, we have turned our attention to rare-earth doped lutetium oxide (Lu_2O_3) nanocrystals[9−11] since it has been observed that when comparing the emission properties of Y- and Lu-containing oxide and fluoride crystals stronger luminescence is observed for the Lu−containing crystals.[12,13] An explanation for this behavior can be found in the results of Guillot-Noël et al.[14] The authors attributed the increase in oscillator strength in related crystals to an intensity-borrowing mechanism that mixes the 4f and 5d lanthanide orbitals via the lattice valence band levels. In YVO_4 for example, these valence band energy levels are due predominantly to the oxygen 2p.

Recent XPS measurements on $LuVO_4$ and various kinds of materials for scintillator applications such as $LuAlO_3$ and Lu_2SiO_5 have shown that the top of the valence band would be more characteristic of lutetium 4f levels.[15,16] This means that the intensity-borrowing mechanism mentioned above could be further enhanced because of an increasing hybridization of the Eu^{3+} and Lu^{3+} 4f orbitals.[15] Thus, lutetium could be a more favorable cation than yttrium for lanthanide dopant emission.

Nanocrystalline Lu_2O_3 doped with lanthanides has garnered much attention recently for use as X-ray scintillators and/or potential phosphors. Zych et al. have examined Eu^{3+} doped Lu_2O_3 synthesized by a combustion technique using urea as the fuel for these potential uses.[17−19] These materials are attractive for X-ray scintillators because of the high density of Lu_2O_3 and the high atomic number of Lu.[20] Furthermore, micrometer sized Y_2O_3:Eu^{3+} phosphor, which is isostructural to Lu_2O_3, has been used since the 1970s as the red component in television projection tubes and fluorescent lighting devices.[21]

In this paper, we present a detailed examination of the luminescent properties of cubic nanocrystalline Lu_2O_3 doped with 1 mol % Eu^{3+} synthesized via a combustion synthesis technique utilizing glycine as the fuel. These results are compared to a cubic bulk Lu_2O_3 doped with 1 mol % Eu^{3+} sample synthesized using a traditional ceramic technique with crystallite sizes in the micron range.

2. Experimental Section

2.1. Samples Preparation. Nanosized Lu_2O_3 crystals of composition $Lu_{1.98}Eu_{0.02}O_3$ were prepared using a solution

* To whom correspondence should be addressed. Address: Department of Chemistry and Biochemistry, Concordia University, 7141 Sherbrooke St. W., Montreal, Canada H4B 1R6. Telephone: +1-514-848-2424 ext. 3350. Fax +1-514-848-2868. E-mail capo@vax2.concordia.ca.

[†] Concordia University.

[‡] Università di Verona, and INSTM.

10.1021/jp0480504 CCC: $27.50
Published on Web 11/02/2004

combustion synthesis procedure.[22,23] The synthesis reaction is

$$6\ M(NO_3)_3 + 10\ NH_2CH_2COOH + 18\ O_2 \rightarrow 3\ M_2O_3 + 5\ N_2 + 18\ NO_2 + 20\ CO_2 + 25\ H_2O$$

where M = Lu, Eu. A glycine-to-metal nitrate molar ratio of 1.2:1 was employed to prepare the precursor solution resulting in a flame temperature of approximately 1200 °C. After the combustion, the powders were fired for 1 h at 500 °C in order to decompose the residual nitrate ions. A thorough structural analysis of the material obtained showed that the average crystallite size is 50 nm[11] and therefore larger than the size of the yttria nanocrystals obtained using the same conditions (about 10−20 nm).[24]

For comparison purposes, a bulk sample of the same composition as the nanocrystalline one was prepared by intimately mixing Eu_2O_3 (Aldrich, 99.99%) and Lu_2O_3 (Aldrich, 99.99+ %), pressing the powders into pellets under a load of 10^3 kg and firing them in air at 1500 °C for 48 h. At this temperature, the optimum homogeneity was obtained.

All lutetia samples were kept in air without any further precaution.

2.2. Emission Spectroscopy. Luminescence spectra were measured by exciting at 257.25 nm using a Coherent model 440 Ultraviolet Generator which frequency doubled the 514.5 nm line of a Coherent Sabre Innova, 20 W argon laser. Site selective spectroscopy was performed using 580.5 or 582.5 nm radiation from a Spectra-Physics 375 tuneable dye-laser operating with Rhodamine 6G (Exciton) pumped by the 514 nm line of the argon laser. The visible emissions were then collected and dispersed using a Jarrell-Ash 1-meter Czerny Turner double monochromator. The signals were monitored with a thermoelectrically cooled Hamamatsu R943-02 photomultiplier tube. A preamplifier, model SR440 Stanford Research Systems, processed the photomultiplier signals, and a gated photon counter model SR400 Stanford Research Systems data acquisition system was used as an interface between the computer and the spectroscopic hardware. The signal was recorded under computer control using the Stanford SR465 software data acquisition/analyzer system.

All low-temperature spectra were obtained using a Janis Research ST-VP-4 continuous flow cryostat with the temperature being monitored by a LakeShore model 330 controller.

2.3. Decay Times Measurements. Luminescence decay times were measured at each of the excitation wavelengths by modulating the excitation laser beam with a Stanford Research Systems optical chopper (model SR540). The photon counter was triggered by a photodiode synchronized by the laser pulse. They were recorded using the same detection equipment and gated photon counter mentioned above.

3. Results and Discussion

3.1. Luminescence Spectroscopy. The sesquioxide Lu_2O_3 is isostructural to Y_2O_3 and crystallizes in a cubic bixbyite structure with space group Ia3.[25] In this lattice, two distinct sites are available for rare earth ions, one with point group symmetry C_2 and the other with point group symmetry C_{3i}, which occur in a 3:1 ratio, respectively. It was reported recently by some of us that the Eu^{3+} ions occupy both these sites in a statistical way for the nanocrystalline sample similar to what is observed for bulk crystals.[26] The presence of Eu^{3+} ions in both sites is reflected in the luminescent and spectral properties of the material. A phonon assisted energy transfer mechanism that occurs between the Eu^{3+} ions residing in the two sites has been studied by Buijs et al.[27]

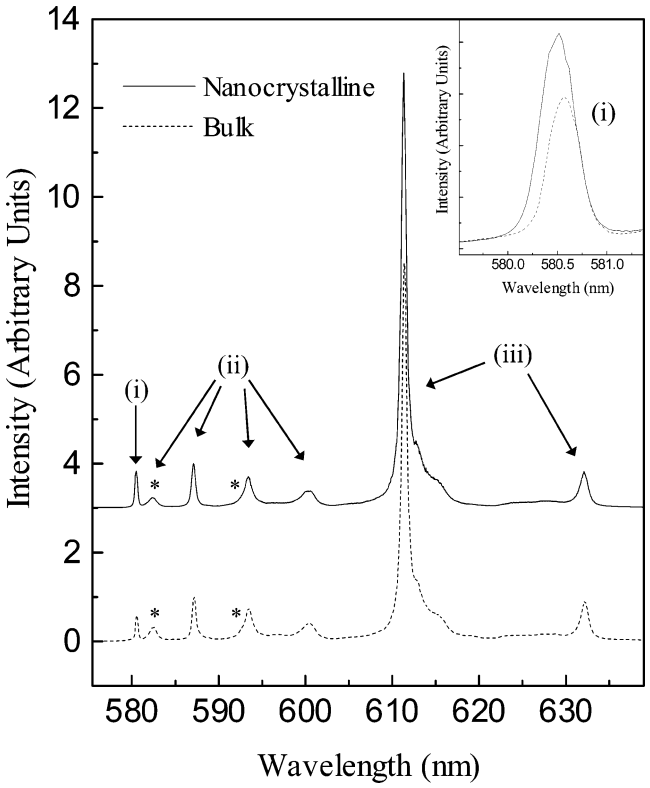

Figure 1. Room-temperature orange-red luminescence of bulk and nanocrystalline Lu_2O_3:Eu^{3+} 1 mol % upon excitation at 257.25 nm. (i) $^5D_0 \rightarrow {}^7F_0$, (ii) $^5D_0 \rightarrow {}^7F_1$, and (iii) $^5D_0 \rightarrow {}^7F_2$ (C_{3i} emissions are noted by ∗.)

The observed optical transitions within the $4f^n$ configuration are mainly attributed to electric dipole transitions, which are forced by the odd parity components of the crystalline electric field. For C_{3i} symmetry, only magnetic dipole transitions should be observed. For the $^5D_0 \rightarrow {}^7F_1$ transition of the Eu^{3+} ion in the cubic bixbyite structure, five emission peaks should be present: two peaks that are attributed to Eu^{3+} ions residing in C_{3i} sites and three peaks for Eu^{3+} in C_2 sites. These peaks have been assigned on the basis of their different emission decay times.[28] Of the two possible radiative decay mechanisms, forced electric dipole and magnetic dipole, only the latter will occur for Eu^{3+} ions in C_{3i} sites thus resulting in a longer decay time.

After excitation into the $Eu^{3+}-O^{2-}$ charge-transfer band with 257.25 nm radiation at room temperature, emission can be observed in the orange-red region of the spectrum resulting from the $^5D_0 \rightarrow {}^7F_0$, $^7F_1$, $^7F_2$ transitions. The UV radiation is absorbed by the charge-transfer band of the Eu^{3+} ion. The ion then nonradiatively decays to lower $4f^n$ levels with the majority of the luminescence occurring from the $^5D_0$ state of the Eu^{3+} ion. The room-temperature luminescence spectra of bulk and nanocrystalline Lu_2O_3:Eu 1 mol % are shown in Figure 1. Assignment of the individual peaks to their corresponding transitions was performed based on data obtained previously for Lu_2O_3:Eu^{3+},[18,29] published data on the isostructural material Y_2O_3:Eu^{3+},[30] luminescence decay times of the individual peaks, time-resolved spectroscopy, and site-selective spectroscopy (see below). Table 1 lists the room temperature and 78 K transition energies found for the Eu^{3+} ion located in the C_2 and C_{3i} sites of the Lu_2O_3 bulk and nanocrystalline materials.

These transitions energies for both samples differ from those reported by Zych et al. in several other studies.[17−19] In the papers

TABLE 1: Observed Transition Energies from the Emission Spectra of Bulk and Nanocrystalline Lu_2O_3:Eu^{3+} 1 mol % at RT and 78 K[a]

	transition energy (cm^{-1})			
	bulk sample		nanocrystalline sample	
transition	RT	78 K	RT	78 K
$^5D_0 \rightarrow {}^7F_0$	17224	17217	17226	17215
$^5D_0 \rightarrow {}^7F_1$	17166*, 17032, 16864*, 16850, 16652	17171*, 17025, 16866*, 16848, 16659	17170*, 17032, 16871*, 16850, 16652	17169*, 17024, 16868*, 16846, 16655
$^5D_0 \rightarrow {}^7F_2$	16358, 16319, 15818	16358, 16314, 16256, 15814	16356, 16318, 16270, 15818	16356, 16315, 16254, 15811

[a] The asterisk (*) denotes emission from Eu^{3+} ion residing in C_{3i} site.

published by Zych et al., the energies reported for the $^5D_0 \rightarrow {}^7F_J$ transitions vary among the numerous publications. The authors offer no explanation for these differences. The differences noted between our transition energies and those reported by Zych may arise from the fact our crystallite sizes are approximately three to four times larger, probably due to the slightly differences in the preparation methods. Difference in the crystallite sizes may induce changes in the crystal field experienced by the Eu^{3+} ion as a larger percentage of the dopant ions would reside on or toward the surface of the nanocrystals resulting in small line shifts between the two samples.

The emission spectra also reveal changes in the relative intensities and line widths of the $^5D_0 \rightarrow {}^7F_0$, $^7F_1$, $^7F_2$ transitions between the bulk and nanocrystalline samples. The inset of Figure 1 clearly shows that the unsplit $^5D_0 \rightarrow {}^7F_0$ line, attributed to Eu^{3+} ions in the C_2 site, in the nanocrystalline sample is significantly broader than in the bulk; indicating a higher disorder of the Eu^{3+} crystalline environment. It is also observed in the nanocrystalline sample that the relative intensity of the $^5D_0 \rightarrow {}^7F_0$ and the hypersensitive $^5D_0 \rightarrow {}^7F_2$ peaks compared to the $^5D_0 \rightarrow {}^7F_1$ peaks are higher than for the bulk. The ratio of the integrate intensities of the $^5D_0 \rightarrow {}^7F_2$ and $^5D_0 \rightarrow {}^7F_1$ transitions under UV excitation

$$R = \frac{I(^5D_0 \rightarrow {}^7F_2)}{I(^5D_0 \rightarrow {}^7F_1)} \quad (1)$$

can be considered indicative of the asymmetry of the coordination polyhedron of the Eu^{3+} ion.[31] The values of the asymmetry ratio R are 3.8 and 4.4 for the bulk and nanocrystalline samples, respectively. These values are slightly smaller than those observed previously in bulk and nanocrystalline $Y_{1.98}Eu_{0.02}O_3$ prepared by wet chemical synthesis.[32] In the case of $Lu_{1.98}Eu_{0.02}O_3$, the R value is again markedly higher for the nanocrystalline sample, suggesting a more distorted local environment for the Eu^{3+} ion than the corresponding bulk sample as the intensity of the $^5D_0 \rightarrow {}^7F_2$ transition strongly depends on the asymmetry of the Eu^{3+} site.[33] This again confirms that a larger portion of the Eu^{3+} ions resides near or at the surface of the nanocrystals due to their higher surface/volume ratio when compared to the bulk material.

The luminescence spectra of the nanocrystalline and bulk samples in the 570−610 nm region upon 257.25 nm excitation at 78 K are shown in Figure 2. When comparing the low-temperature spectra of both samples to their corresponding RT spectra, several changes are observed. Most obvious is the reduction in the emission line widths as one reaches 78 K due to a reduction in electron−phonon coupling. Also noticeable are a small wavelength shift in several of the emission peaks with decreasing temperature along with a change in the relative intensities of the 587 and 582.5 nm peaks. To illustrate these changes, the luminescence of the nanocrystalline Lu_2O_3:Eu^{3+} 1 mol % at RT and 78 K under UV excitation is shown in Figure 3.

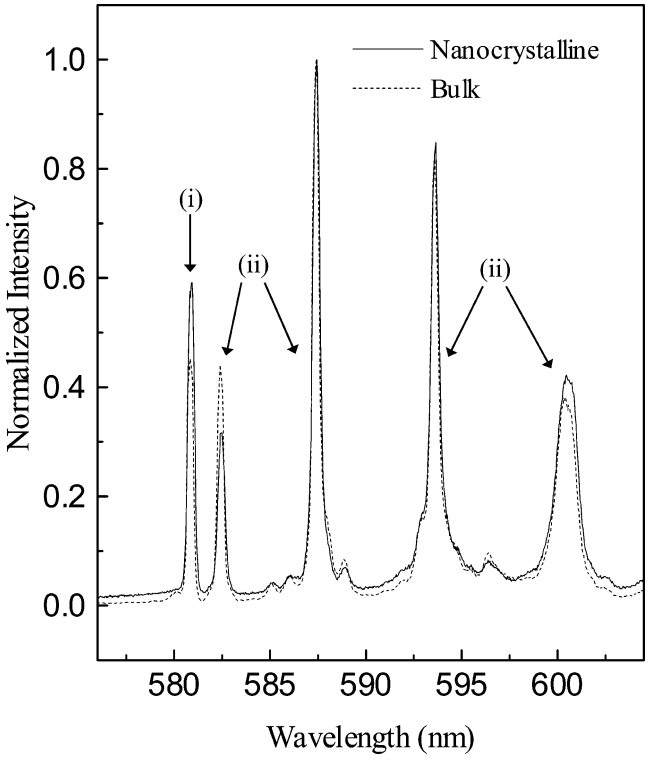

Figure 2. Detailed structure of $^5D_0 \rightarrow {}^7F_0$, $^7F_1$ luminescence of bulk and nanocrystalline Lu_2O_3:Eu^{3+} 1 mol % at 78 K (λ_{exc} = 257.25 nm). (i) $^5D_0 \rightarrow {}^7F_0$ and (ii) $^5D_0 \rightarrow {}^7F_1$.

Several theoretical and experimental studies[34,35] have examined how changes in electron−phonon coupling with temperature affect peak positions and widths. The majority of these studies have ignored changes in the crystal structure with temperature since these were assumed to be insignificant in the systems studied. Recently, it has been found that changes in the peak positions with decreasing temperature in cubic Eu_2O_3 can be attributed not only to differences in the electron−phonon coupling strength at low temperature but also to changes that occur in the crystal structure due to thermal effects.[36] Thus, it is safe to assume that the observed Eu^{3+} transition energy changes in the isostructural Lu_2O_3 with temperature are due to changes in both the electron−phonon coupling and crystal structure.

It is also noticeable in Figures 1−3 that the 580 nm ($^5D_0 \rightarrow {}^7F_0$) shifts to different extents with temperature change when comparing the nanocrystalline to bulk samples. It is observed that the line shift is more pronounced in the case of the nanocrystalline sample. As mentioned above the temperature shift of the luminescence is ascribed to a temperature-derived contribution (linked to the electron−phonon coupling) and a

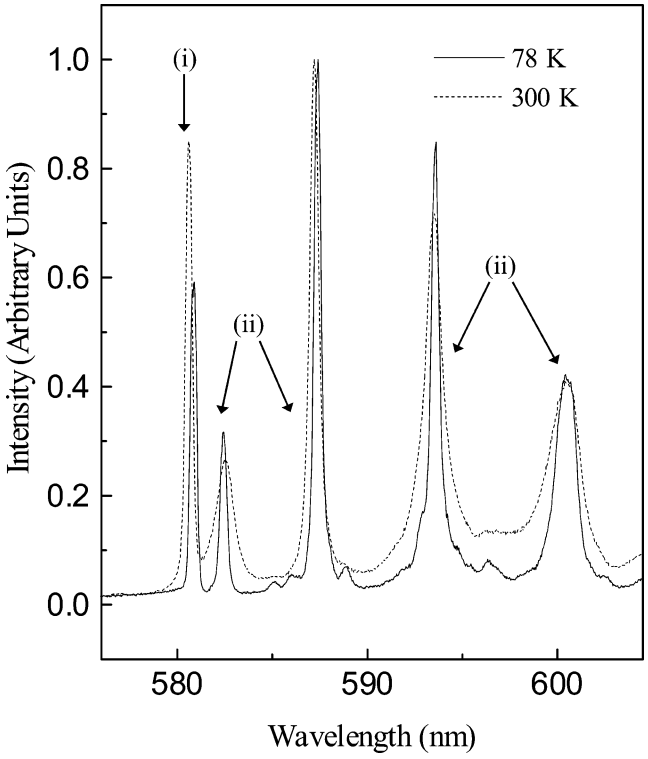

Figure 3. Detailed structure of $^5D_0 \rightarrow {}^7F_0$, $^7F_1$ luminescence of nanocrystalline Lu_2O_3:Eu^{3+} 1 mol % at RT and 78 K ($\lambda_{exc} = 257.25$ nm). (i) $^5D_0 \rightarrow {}^7F_0$ and (ii) $^5D_0 \rightarrow {}^7F_1$.

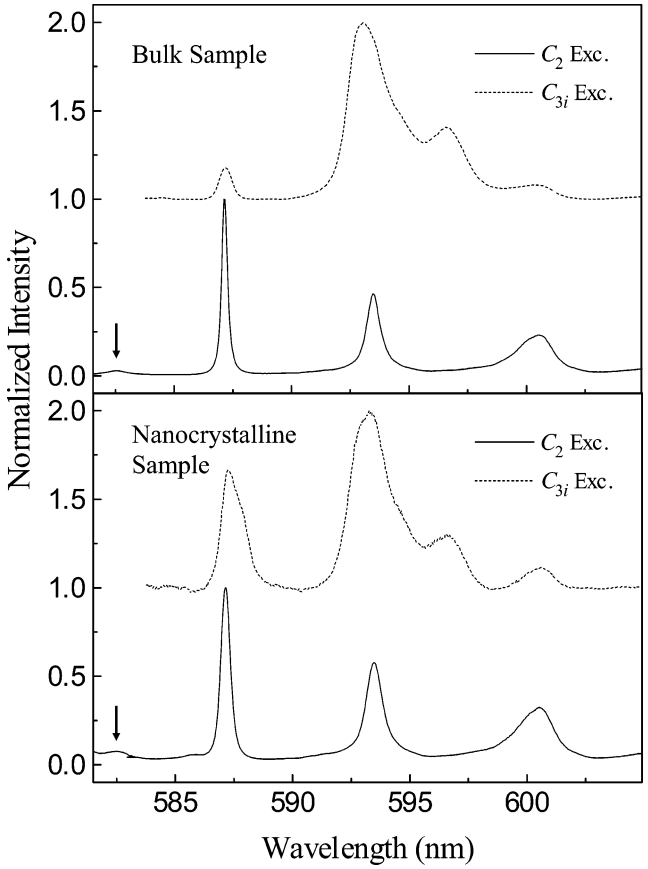

Figure 4. Emission spectra $^5D_0 \rightarrow {}^7F_1$ for selective excitation into the $^5D_0$ level (C_2 Exc. − 580.5 nm, C_{3i} Exc. 582.5 nm) of bulk and nanocrystalline Lu_2O_3:Eu^{3+} 1 mol % at RT. Note the presence of weak C_{3i} peak at 582.5 nm in both spectra obtained under C_2 excitation (marked with an arrow).

volume-derived contribution (linked to the thermal expansion, leading to a change in the equilibrium atomic positions, and therefore in the crystal field).[36] To distinguish between these two contributions, one should perform spectroscopic measurements as a function of the pressure and temperature. It is possible that the presence of varying amounts of these contributions between the two types of samples can explain the difference in the degree of line shift with temperature. At this time though, a precise explanation is clearly outside the scope of the paper.

3.2. Site-Selective Spectroscopy. Besides examining the luminescence decay times of the Eu^{3+} ions in differing sites, it is possible to elucidate bands which originate from the two different sites by comparing the luminescence spectra under excitation into each separate excitation band. Under excitation into a Eu^{3+} (C_{3i}) transition only C_{3i} lines should appear in the luminescence spectra if one neglects the effects of energy transfer between the two sites. As such, the reverse should also hold true for excitation into Eu^{3+} (C_2) transition. This type of site selective spectroscopy is also a powerful tool for examining the energy transfer mechanism that occurs between the Eu^{3+} ions in the two sites.

Upon excitation at room temperature into the $^7F_0 \rightarrow {}^5D_0$ (C_2) transition, peaks are visible in the orange-red emission spectra of both samples that originate from Eu^{3+} ions in C_2 and C_{3i} sites as seen in Figure 4. Emission is observed from the corresponding $^5D_0 \rightarrow {}^7F_1$, $^7F_2$ transitions for the C_2 site. A weak emission line at 582.4 nm [$^5D_0$ (C_{3i}) $\rightarrow {}^7F_1$ (C_{3i})] confirms the presence of a weak energy transfer from $^5D_0$ (C_2) to the $^5D_0$ (C_{3i}) level over the energy gap separating the two states. Nevertheless, the majority of the exciting energy is still being released as C_2 type emissions. Likewise, room-temperature emission is seen originating from both the C_2 and C_{3i} sites under C_{3i} excitation at 582.4 nm. Emission is observed from the corresponding $^5D_0 \rightarrow {}^7F_1$, $^7F_2$ transitions for the C_2 site along with the presence of a C_{3i} transition at 592.9 nm and a vibronic transition of C_{3i} character at 597 nm. Thus, at room temperature, there is effective energy transfer from the Eu^{3+} ions in C_{3i} to C_2 sites and also a less efficient energy transfer from C_2 to C_{3i} sites similar to what was observed by Zych for the same material.[18] It is clear though from comparing the spectra obtained under C_{3i} excitation to those obtained under nonselective UV excitation that a higher percentage of the exciting energy is being released as C_{3i} type emissions in the selective excitation case even with the presence of the energy transfer mechanism. This experimental data also indicates that the energy transfer between the C_{3i} and C_2 sites must occur at the $^5D_0$ level even for nonselective UV excitation.

The orange-red emission spectra of the 1 mol % doped bulk and nanocrystalline samples under $^7F_0 \rightarrow {}^5D_0$ (C_2) excitation at 78 K are shown in Figure 5. It is evident from the spectra by the absence of C_{3i} emissions that the C_2 to C_{3i} energy transfer process is to a great extent reduced at this temperature as it is a thermally activated process.[18] The spectra now consist only of C_2 type emission lines from the corresponding $^5D_0 \rightarrow {}^7F_1$, $^7F_2$ transitions. The reverse is not true though for $^7F_0 \rightarrow {}^5D_1$ (C_{3i}) excitation at 78 K shown in the same figures. Here C_2 type emission is still observed from the $^5D_0 \rightarrow {}^7F_1$, $^7F_2$ transitions in both the bulk and nanocrystalline samples indicating the C_{3i} to C_2 energy transfer process is effective even at 78 K.

3.3. Luminescence Decay Times. Table 2 reports the luminescence decay times of the $^5D_0 \rightarrow {}^7F_1$ and $^5D_0 \rightarrow {}^7F_2$ transitions under various excitation wavelengths. All decay curves exhibited single-exponential behavior unless otherwise stated, similar to what has been reported in the past for these

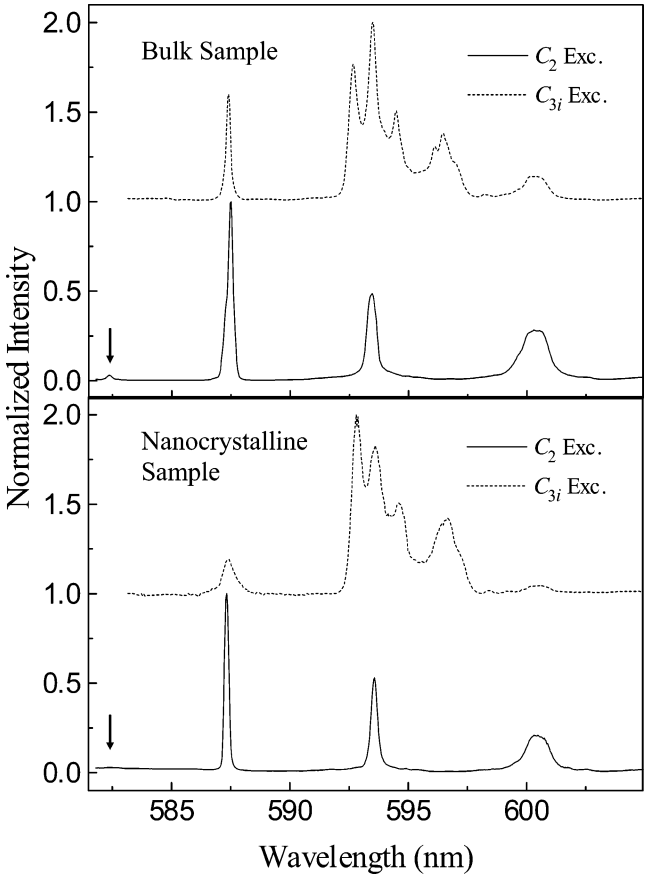

Figure 5. Emission spectra $^5D_0 \rightarrow {}^7F_1$ for selective excitation into the $^5D_0$ level (C_2 Exc. − 580.5 nm, C_{3i} Exc. 582.5 nm) of bulk and nanocrystalline Lu_2O_3:Eu^{3+} 1 mol % at 78 K. Note the presence of weak C_{3i} peak at 582.5 nm in both spectra obtained under C_2 excitation (marked with arrow).

TABLE 2: $^5D_0$ Luminescence Decay Times for Bulk and Nanocrystalline Lu_2O_3:Eu^{3+} 1 Mol % at RT and 78 K (λ_{Exc} = 257.25 Nm)

sample	temp (K)	emission wavelength (nm)	emitting level and site symmetry	decay time (ms)
bulk	RT	611	$^5D_0$ (C_2)	1.0
bulk	RT	582.4	$^5D_0$ (C_{3i})	4.4
bulk	78	611	$^5D_0$ (C_2)	1.1
bulk	78	582.4	$^5D_0$ (C_{3i})	6.0
nano	RT	611	$^5D_0$ (C_2)	2.0
nano	RT	582.4	$^5D_0$ (C_{3i})	8.7
nano	78	611	$^5D_0$ (C_2)	2.3
nano	78	582.4	$^5D_0$ (C_{3i})	17

transitions in bulk and nanocrystalline Lu_2O_3 with identical doping levels.[17,37] On examining the values of the luminescence decay times of the nanocrystalline and bulk samples under UV excitation, one notices a lengthening of the decay time in the nanocrystalline sample, for both the room temperature and 78 K measurements. This behavior has been explained by Meltzer et al.[38] on the basis of changes in the refractive index of the surrounding medium of the Eu^{3+} ion as one goes to the nanometer size range.

The radiative lifetime of electric dipole transitions of an ion embedded in a medium may be expressed by the formula[39]

$$\tau_R \sim \frac{1}{f(\mathrm{ED})} \frac{\lambda_0^2}{\left[\frac{1}{3}(n^2+2)\right]^2 n} \qquad (2)$$

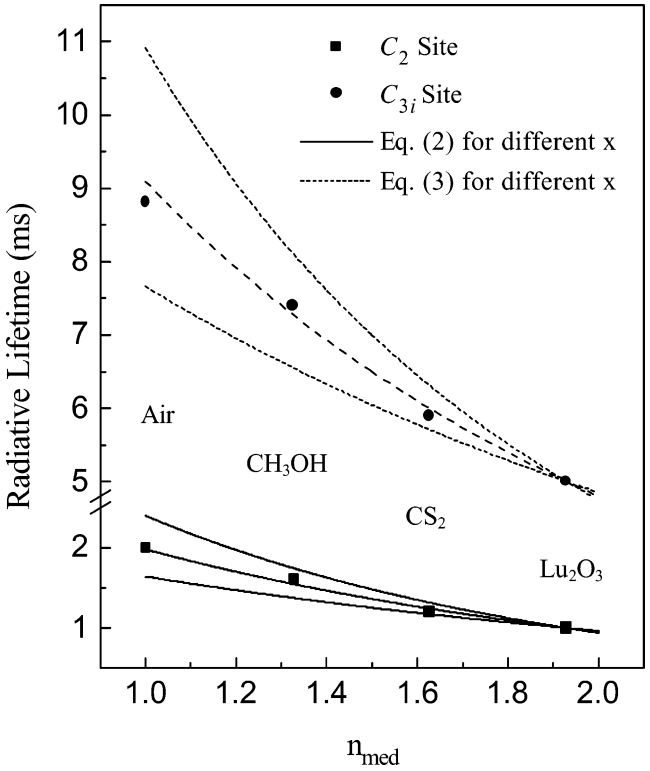

Figure 6. Dependence of the $^5D_0$ lifetime for the Eu^{3+} C_2 and C_{3i} sites on the index of refraction of the media n_{med} at T = 298 K.

where f(ED) is the oscillator strength for the electric dipole transition, λ_0 is the wavelength in a vacuum, and n is the refractive index of the medium. An analogous formula can be found for magnetic dipole transitions[39]

$$\tau_R \sim \frac{1}{f(\mathrm{MD})} \frac{\lambda_0^2}{n^3} \qquad (3)$$

where f(MD) is the oscillator strength for the magnetic dipole transition, λ_0 is the wavelength in a vacuum, and n is the refractive index of the medium. It was observed in monoclinic Y_2O_3:Eu^{3+} that the radiative lifetime of an electronic transition of an ion embedded in a medium is correlated with an effective refractive index n_{eff}, which is a function of the refractive index of yttria and the fraction of space occupied by the nanoparticles surrounded by the media with refractive index n_{med}.[38] The effective refractive index is given by

$$n_{eff}(x) = x \cdot n_{Lu_2O_3} + (1-x) \cdot n_{med} \qquad (4)$$

where x is the "filling factor" showing what fraction of space is occupied by the nanoparticles. One may replace n by n_{eff} when the average size of the particles in questions much smaller than the wavelength of light, as is the case for the nanocrystalline lutetia under investigation.

We have performed similar experiments on the nanocrystalline Eu^{3+} doped Lu_2O_3 and have found comparable results. In Figure 6, the lifetime at room temperature of the $^5D_0$ state of Eu^{3+} for both the C_2 and C_{3i} sites are plotted versus the refractive index of the media (n_{med}) in which the nanoparticles are dispersed. The experimental data for both the C_2 and C_{3i} sites have been used for fitting with eqs 1 and 2, respectively, using x as an adjustable parameter. In both the C_2 and C_{3i} sites, it was found that a filling factor of 0.625 gave a reasonable fit (see Figure 6). Results using x = 0.525 and 0.725 are shown

by the other curves. Thus, as the refractive index of lutetia[40] is 1.93, a lengthening of the decay times of the electronic levels of Eu^{3+} for the nanoparticles in air is expected, in agreement with the present results.

This is the first time that this procedure has been performed for the Eu^{3+} C_{3i} decay. The fact that the same filling factor was determined for both the C_2 and C_{3i} decays is a good indication that this fitting procedure is a valid one. To validate the results further, a corresponding bulk sample was ground with a mortar and pestle and placed immersed in the various solvents utilized. No changes in the bulk C_2 or C_{3i} decay time were observed under these conditions.

At 78 K, the lifetime of the $^5D_0$ (C_2) level under UV excitation was observed to increases from 1.0 to 1.1 ms for the bulk sample. A similar increase from 2.0 to 2.3 ms was also found in the nanocrystalline sample. A more striking increase was observed in the lifetime of the $^5D_0$ (C_{3i}) level at 78 K, where the lifetimes of both samples were approximately double of what was observed at room temperature (Table 2). We propose that the lengthening of the lifetime of these levels are primarily due to the reduction of both the C_2 to C_{3i} and C_{3i} to C_2 energy transfer mechanisms between Eu^{3+} ions at low temperature. Since the major pathway for nonradiative relaxation for Eu^{3+} in Lu_2O_3 is energy transfer among the Eu^{3+} ions to a quenching center, if the energy transfer process is less efficient at low temperatures then these nonradiative processes will be reduced and the lifetime of the level will increase. In the case of the $^5D_0$ (C_{3i}) level at RT, the lifetime is shortened by energy-transfer to Eu^{3+} ions residing in C_2 sites which possess significantly shorter lifetime. At 78 K, the probability for the downward energy-transfer from the C_{3i} to C_2 site is decreased; reducing this pathway for relaxation and resulting in the significant increase of the $^5D_0$ (C_{3i}) lifetime.

3.4. Judd-Ofelt Parameters. To gain more insight into the possible structural changes surrounding the Eu^{3+} ion between the two samples, the experimental intensity parameters Ω_2 and Ω_4 were calculated from the emission spectra using a technique developed by Porcher[41] and subsequently used by others.[42] This technique takes advantage of the fact that the intensities of the $^5D_0 \rightarrow {}^7F_2$, $^5D_0 \rightarrow {}^7F_4$, and $^5D_0 \rightarrow {}^7F_6$ transitions are solely dependent on the Ω_2, Ω_4, and Ω_6 parameters, respectively. Also, the $^5D_0 \rightarrow {}^7F_1$ transition possesses solely magnetic dipole character, whereas the other $^5D_0 \rightarrow {}^7F_J$ transitions are purely electric dipole.

It is possible to express the spontaneous emission intensity for an $i \rightarrow k$ transition as[43]

$$I(i,k) = \hbar\omega_{ik} A(i,k) N(i) \tag{5}$$

where $\hbar\omega_{ik}$ is the transition energy, $N(i)$ is the population of the emitting state and $A(i,k)$ is the spontaneous emission probability for the $i \rightarrow k$ transition. In the case of the $^5D_0 \rightarrow {}^7F_J$ emission transitions of the Eu^{3+} ion, the value of $A(^5D_0, {}^7F_J)$ can be determined from the equation[44]

$$A(^5D_0, {}^5F_J) = \frac{4e^2\omega^3}{3\hbar c^3}\chi \sum_{\lambda} \Omega_\lambda \langle {}^7F_J || U^{(\lambda)} || {}^5D_0 \rangle^2 \tag{6}$$

where $\chi = n_0(n_0^2 + 2)^2/9$ is the Lorentz local field correction and n_0 is the index of refraction of the host. For the nanocrystalline sample, we replace n_0 with the n_{eff} refractive index determined in the previous section. The reduced matrix elements were taken from Carnall et al.[45]

TABLE 3: Ω_λ, Judd-Ofelt Intensity Parameters for the Nanocrystalline and Bulk Lu_2O_3:Eu^{3+} 1 mol %; R_{02}, Ratio between the Emission Intensities of the $^5D_0 \rightarrow {}^7F_0$ and $^5D_0 \rightarrow {}^7F_2$ Transitions

sample	Ω_2 (10^{-20} cm^2)	Ω_4 (10^{-20} cm^2)	R_{02}
bulk	6.14	1.71	0.019
nanocrystalline	9.07	2.60	0.025

The calculated values of the Judd-Ofelt parameters are given in Table 3 for both the nanocrystalline and bulk samples. The Ω_λ parameters for the lanthanide ion are noticeably higher for the nanocrystalline sample than in the bulk. This behavior could be due to the fact that for the nanocrystalline host a higher fraction of the Eu^{3+} ions is on the surface of the particles with respect to the bulk one and therefore the average crystal field experienced by the ions in the nanoparticles is different with respect to that for the bulk sample. Moreover, it has been shown that adsorbed CO_2 and water are present as contaminants at the surface of the Lu_2O_3 nanoparticles,[10] and therefore, they could contribute to vary the crystal field experienced by the Eu^{3+} ion. In particular, changes in the Ω_2 value can be related to changes in the structural environment around the rare earth ion due to the hypersensitivity of the $^5D_0 \rightarrow {}^7F_2$ transition. The larger Ω_2 parameter in the nanocrystalline sample is a good indication that the symmetry of the Eu^{3+} sites is distorted compared to the bulk sample due to the samples small size.

Another useful value to examine is the ratio of the emission intensities of the $^5D_0 \rightarrow {}^7F_0$ to $^5D_0 \rightarrow {}^7F_2$ transitions R_{02}. This parameter can give information about the J-mixing effect related with the $^5D_0 \rightarrow {}^7F_0$ transition.[42] As with the Ω_k values, the R_{02} ratio was found to be higher for the nanocrystalline sample reflecting a larger J-mixing. This indicates that in the nanocrystalline sample the structure environment around the Eu^{3+} ions is of higher complexity compared to the bulk.

Conclusions

Emission spectra and lifetimes of the excited states of the nanocrystal samples were found to differ significantly from those of the bulk. Judd-Ofelt intensity parameters calculated from the emission spectra of the samples indicate that the Eu^{3+} sites in the nanocrystalline sample are more disordered compared to the bulk sample. A higher R_{02} ratio confirms that the Eu^{3+} environment in the nanocrystalline sample is more complex than in the bulk. The longer lifetimes for the $^5D_0$ excited state were successfully attributed to a modification in the refractive index for the nanocrystalline material. By fitting the decay curves for both the C_2 and C_{3i} sites, it was found that the nanocrystals have a filling factor of 0.625.

Acknowledgment. The authors gratefully acknowledge the Natural Science and Engineering Research Council of Canada and MURST (Project 9903222581_005) of Italy, for financial support. The authors gratefully thank Erica Viviani (Università di Verona) for expert technical assistance.

References and Notes

(1) Williams, D. K.; Yuan, H.; Tissue, B. M. *J. Lumin.* **1999**, *83−84*, 297−300.

(2) Shea, L. E.; McKittrick, J.; Lopez, O. A. *J. Am. Ceram. Soc.* **1996**, *79*, 3257−3265.

(3) Tissue, B. M. *Chem. Mater.* **1998**, *10*, 2837−2845.

(4) Eilers, H.; Tissue, B. M. *Chem. Phys. Lett.* **1996**, *251*, 74−78.

(5) Williams, D. K.; Bihari, B.; Tissue, B. M.; McHale, J. M. *J. Phys. Chem. B* **1998**, *102*, 916−920.

(6) Capobianco, J. A.; Boyer, J. C.; Vetrone, F.; Bettinelli, M.; Speghini, A. *Chem. Mater.* **2002**, *14*, 2915−2921.

(7) Vetrone, F.; Boyer, J. C.; Capobianco, J. A.; Speghini, A.; Bettinelli, M. *Chem. Mater.* **2003**, *15*, 2737−2743.
(8) Vetrone, F.; Boyer, J. C.; Capobianco, J. A.; Speghini, A.; Bettinelli, M. *Nanotechnology* **2004**, *15*, 75−81.
(9) Vetrone, F.; Boyer, J. C.; Capobianco, J. A.; Speghini, A.; Bettinelli, M. *J. Phys. Chem. B* **2002**, *106*, 5622−5628.
(10) Capobianco, J. A.; Vetrone, F.; Boyer, J. C.; Speghini, A.; Bettinelli, M. *Opt. Mater.* **2002**, *19*, 259−268.
(11) Polizzi, S.; Bucella, S.; Speghini, A.; Vetrone, F.; Naccache, R.; Boyer, J. C.; Capobianco, J. A. *Chem. Mater.* **2004**, *16*, 1330−1335.
(12) Laroche, M.; Girard, S.; Moncorgé, R.; Bettinelli, M.; Abdulsabirov, R.; Semashko, V. *Opt. Mater.* **2003**, *22*, 147−154.
(13) Rambaldi, P.; Moncorgé, R.; Wolf, J. P.; Pédrini, C.; Gesland, J. Y. *Optics Commun.* **1998**, *146*, 163−166.
(14) Guillot-Noel, O.; Bellamy, B.; Viana, B.; Gourier, D. *Phys. Rev. B* **1999**, *66*, 1668−1677.
(15) Maunier, C.; Doualan, J. L.; Moncorgé, R.; Speghini, A.; Bettinelli, M.; Cavalli, E. *J. Opt. Soc. Am. B* **2002**, *19*, 1794−1800.
(16) Moine, B.; Dujardin, C.; Lautesse, H.; Pedrini, C.; Combes, C. M.; Belski, A.; Martin, P.; Gesland, J. Y. *Mater. Sci. Forum* **1997**, *239*−*241*, 245−248.
(17) Zych, E.; Hreniak, D.; Strek, W. *J. Phys. Chem. B* **2002**, *106*, 3805−3812.
(18) Zych, E. *J. Phys.: Condens. Matter* **2002**, *14*, 5637−5650.
(19) Zych, E. *J. Alloys Compd.* **2002**, *344*, 332−336.
(20) Lempicki, A.; Brecher, C.; Szupryczynski, P.; Lingertat, H.; Nagarkar, V. V.; Tipnis, S. V.; R.Miller, S. *Nucl. Instrum. Methods Phys. Res., Sect. A* **2002**, *488*, 579−590.
(21) Franz, K. A.; Kehr, W. G.; Siggel, A.; Wieczoreck, J. In *Ullman's Encyclopedia of Industrial Chemistry*; Elvers, B., Hawkins, S., Schulz, G., Eds.; VCH Publishers: Weinheim, Germany, 1985; Vol. A15.
(22) Ye, T.; Guiwen, Z.; Weiping, Z.; Shangda, X. *Mater. Res. Bull.* **1997**, *32*, 501−506.
(23) Tessari, G.; Bettinelli, M.; Speghini, A.; Ajò, D.; Pozza, G.; Depero, L. E.; Allieri, B.; Sangaletti, L. *Appl. Surf. Sci.* **1999**, *144*−*145*, 686−689.
(24) Polizzi, S.; Fagherazzi, G.; Battagliarin, M.; Bettinelli, M.; Speghini, A. *J. Mater. Res.* **2001**, *16*, 146−154.
(25) Saiki, A.; Ishizawa, N.; Mizutani, N.; Kato, M. *J. Ceram. Soc. Jpn.* **1985**, *93*, 649−654.
(26) Concas, G.; Spano, G.; Bettinelli, M.; Speghini, A. *Z. Naturforsch., A: Phys. Sci.* **2003**, *58*, 551−557.
(27) Buijs, m.; Meyerink, A.; Blasse, G. *J. Lumin.* **1987**, *37*, 9−20.
(28) Heber, J.; Hellwege, K. H.; Köbler, U.; Murmann, H. *Z. Physik.* **1970**, *237*, 189−204.
(29) Karbowiak, M.; E. Z., Hölsä, J. *J. Phys.: Condens. Matter* **2003**, *15*, 2169−2181.
(30) Leavitt, R. P.; Gruber, J. B.; Chang, N. C.; Morrison, C. A. *J. Chem. Phys.* **1982**, *76*, 4775−4788.
(31) Oomen, E. W. J. L.; Dongen, A. M. A. v. *J. Non-Cryst. Solids* **1989**, *111*, 205−13.
(32) Polizzi, S.; Battagliarin, M.; Bettinelli, M.; Speghini, A.; Fagherazzi, G. *J. Mater. Chem.* **2002**, *12*, 742−747.
(33) Peacock, R. D. *The Intensities of Lanthanide f − f Transitions*; Springer−Verlag: New York, 1975; Vol. 22.
(34) Kashida, T. *Phys. Rev.* **1969**, *185*, 500−508.
(35) Yen, W. M.; Scott, W. C.; Schawlow, A. L. *Phys. Rev.* **1964**, *136*, A271-A283.
(36) Chen, G.; Haire, R. G.; Peterson, J. R. *J. Solid State Chem.* **1993**, *102*, 126−131.
(37) Zych, E.; Karbowiak, M.; Domagala, K.; Hubert, S. *J. Alloys Compd.* **2002**, *341*, 381−384.
(38) Meltzer, R. S.; Feofilov, S. P.; Tissue, B. M.; Yuan, H. B. *Phys. Rev. B.* **1999**, *60*, R14012−R14015.
(39) Henderson, B.; Imbusch, G. F. *Optical Spectroscopy of Inorganic Solids*; Clarendon Press: Oxford, U.K., 1989.
(40) Medenbach, O.; Dettmar, D.; Shannon, R. D.; Fischer, R. X.; Yen, W. M. *J. Opt. A: Pure Appl. Opt.* **2001**, *3*, 174−177.
(41) Huang, J.; Loriers, J.; Porcher, P. *C. R. Acad. Sci., Ser. II* **1982**, *294*, 545−548.
(42) Malta, O. L.; Brito, H. F.; Menezes, J. F. S.; Silva, F. R. G. e.; Jr., S. A.; Jr., F. S. F.; Andrade, A. V. M. d. *J. Lumin.* **1997**, *75*, 255−268.
(43) Thorne, A. P. *Spectrophysics*; 2nd ed.; Chapman and Hall: New York, 1988.
(44) Kodaira, C. A.; Claudia, A.; Brito, H. F.; Felinto, M. C. F. C. *J. Solid State Chem.* **2003**, *171*, 401−407.
(45) Carnall, W. T.; Crosswhite, H.; Crosswhite, H. M. *Energy level structure and transition probabilities in the spectra of the trivalent lanthanides in LaF_3*; Argonne National Laboratory: Argone, IL, 1978.